PROCEEDINGS, 50th Workshop on Geothermal Reservoir Engineering
Stanford University, Stanford, California, February 10-12, 2025
SGP-TR-229

Thermodynamic Modelling of Hydrogen in Hydrothermal Fluids

Marwah Alsinan, Dick Kachuma and Anthony R. Kovscek

367 Panama Street, Stanford, CA 94305

mms22@stanford.edu

Keywords: Hydrogen, Hydrothermal, Gas solubility, Thermodynamics

ABSTRACT

Hydrothermal fluids, produced through interactions between brine and ultramafic rocks at high temperatures, contain hydrogen generated via serpentinization of ultramafic rocks. Understanding hydrogen partitioning between vapor and liquid phases in high salinity fluids is crucial to estimate hydrogen production in these systems.

We reviewed several frameworks for thermodynamic evaluation of hydrogen mixtures starting from a symmetric approach for vapor-liquid equilibria to the asymmetric approach. The asymmetric approach is more popular for studying gas-brine systems because it allows speciation calculations for reactive transport. At conditions near the critical point of water, however, the asymmetric approach needs to be extended to capture the physics of that region accurately.

We compared the performance of three models, including: Helgeson–Kirkham–Flowers (HKF), Akinfiev and Diamond (2003), Plyasunov and Bazrakina (2018) against datasets at near and super-critical conditions and with brine to evaluate the salting-out effect. The Akinfiev and Diamond (2003) and Plyasunov and Bazrakina (2018) models predicted solubilities and Henry's coefficients more accurately compared to the HKF model. As expected, the models were not able to capture the salting-out effect that is of significant impact in the single-phase super-critical region compared to super-critical vapor because salts do not partition in significant amounts to the vapor phase. Our analysis revealed that a Sechenov coefficient between 0.4 to 0.6 captures the salting-out effect up to 1 molal salinity. Additional experiments, however, are required at higher salinities to evaluate salting-out effect at super-critical conditions.

Accurate modeling of thermodynamic properties in the H_2-H_2O-NaCl system is crucial for hydrogen exploration and evaluation of redox conditions in the earth's crust and upper mantle. Also, improved understanding could enhance the economic feasibility of energy extraction systems from geothermal reservoirs and vent fields.

INTRODUCTION

The interaction between saline water and ultramafic rocks deep within the earth generates highly mobile hydrothermal fluids enriched with minerals and various chemical species. For example, hydrogen (H_2) emissions were detected from several vent sites along the Mid-Atlantic Ridge, including Rainbow, Lost City, Logatchev I and II, and Ashadze I and II (Charlou et al. (2010)). In this geological setting, hydrogen is produced through the hydrothermal alteration (oxidation) of ferrous minerals in ultramafic rocks during serpentinization (Klein et al. 2020). The expelled hydrothermal fluids consist of salt-rich brines and salt-poor vapors. Vapor-liquid immiscibility in these systems is indicated by the presence of bubbles in some hydrothermal chimneys. Additionally, because vapor and liquid phases have distinct physical properties (e.g., density, viscosity), they can move independently through the crust and upper mantle. As a result, this partitioning affects the distribution of gases, and particularly H_2, in the crust and upper mantle. Therefore, determining the amount of H_2 produced by these systems requires an understanding of hydrogen partitioning between the vapor and liquid phases in NaCl-rich fluids under high temperature and pressure conditions.

Figure 1 illustrates typical hydrogen molal concentrations in four hydrothermal fluid types, including geothermal fluids, ocean vents, fluid inclusions (e.g., in quartz), and volcanic emissions (adapted from Bazarkina, 2019). Notably, hydrothermal fluids span temperatures from about 80 °C to 1100 °C (353.15 K to 1373.15 K) and cross water's critical temperature (374 °C/647.15 K). Over this broad range, dissolved hydrogen undergoes major changes and this, complicates its thermodynamic modeling.

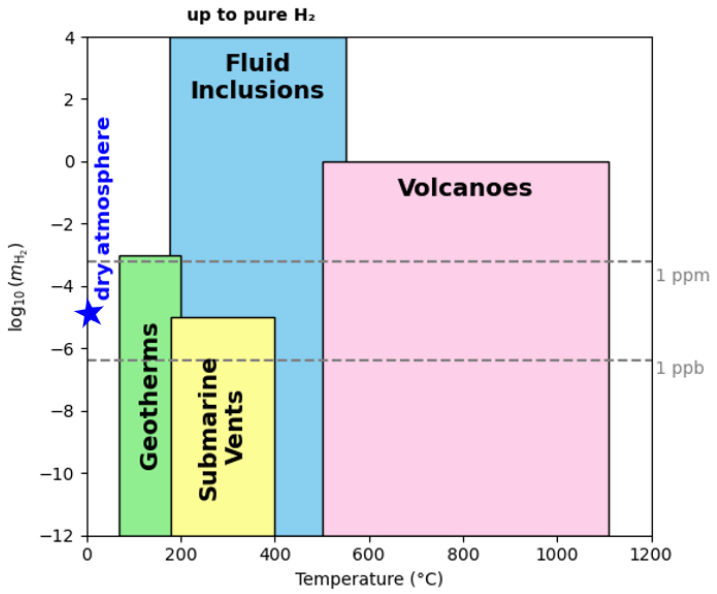

Figure 1: Range of H_2 molality (mol/kg) in brine found naturally in different hydrothermal fluids. Figure adapted from Bazarkina (2019).

Equations of state (EoS) often excel at predicting thermodynamic properties of most gases but can be much less accurate for hydrogen-bearing fluids. This is attributed to hydrogen's exceptionally low critical temperature, a region where quantum effects become significant, rendering ordinary parameter-scaling methods for EoS less reliable. For example, at 2000 MPa and 1000 K, comparing the fugacity coefficient amongs various EoS in the literature, reveals that these approaches have differences of up to 0.45 $\log_{10}$ units (Plyasunov et al., 2018). In contrast, for H_2O under the same conditions, the discrepancy is merely 0.07 $\log_{10}$ units. These observations underscore the need to evaluate and refine existing thermodynamic models for hydrogen solubility and, this is a key goal of the paper.

2. MODELLING HYDROGEN-BRINE EQUILBRIUM

2.1 φ–φ Approach

The most common approach to model vapor-liquid equilibria is through an equation of state (EoS), such as a cubic EoS. Equilibrium may be assessed through Gibbs energy minimization, and leads to the following thermodynamic constraint

$$\mu_{ig} = \mu_{il} \tag{1}$$

where μ is the chemical potential for component *i* and *l* and *g* refer to the liquid and gaseous phases, respectively. The chemical potential is defined as

$$\mu_i = \mu_i^0 + RT\, ln\hat{f}_i \tag{2}$$

where μ° represents the standard molar chemical potential that for gases is defined at 1 bar and the temperature of interest. R is the gas constant, T is temperature, f_i is fugacity of component *i* in the liquid or gas phase and, is needed to predict the chemical potential at non-ideal conditions. The fugacity is defined as

$$\hat{f}_i = x_i P \hat{\emptyset}_i \tag{3}$$

where *x* refers to the liquid or gas molar fraction, *P* is pressure and φ is fugacity coefficient. When substituting the definition of chemical potential (Eqs. 2 and 3) into the thermodynamic constraint in Eq. 1, we obtain the following thermodynamic equilibrium condition for component *i*

$$k = \frac{y_i}{x_i} = \frac{\hat{\varphi}_{il}}{\hat{\varphi}_{ig}} \tag{4}$$

where *k* is the k-value for component *i.*

This φ–φ modeling strategy is widely used because of its simplicity, as it does not require standard-state calculations or adjustments near the critical point. Incorporating polar molecules, however, and electrolytes such as in H_2O-NaCl systems can be difficult, largely due to differences in how salt behaves thermodynamically in the gas versus the liquid phase. Even so, the φ–φ approach has been successfully applied to the H_2–H_2O–NaCl system using the PC-SAFT equation (Kiemde et al., 2023) and advanced Peng–Robinson frameworks, including e-PR-CPA (Chabab et al., 2020) and Soriede–Whitson (Chabab et al., 2024). The latter is popular in oil and gas simulation

software. Nonetheless, extending these models to perform speciation calculations remains challenging because, they do not treat salts as separate components but rather incorporate their effects through binary interaction parameters.

2.2 γ –φ Approach

A hybrid approach is to assign a fugacity coefficient for the component in the gas phase and an activity coefficient, γ, for the aqueous phase. This approach is useful for expanding to speciation calculations such as gas dissolution reaction into water, i.e.

$$A_{gas} \leftrightarrow A_{aq} \tag{5}$$

In this framework, the species chemical potential (μ_i) and activity (a_i) is defined as:

$$\mu_{iaq} = \mu^0_{iaq} + RT\, lna_i = \mu^0_{iaq} + RT\, lnm_i + RT\, ln\, \gamma_i \tag{6}$$

where m_i represents the species molality in the aqueous phase, γ_i is the species activity coefficient in a molality basis and $\mu_i°$ is standard molar chemical potential for the aqueous solutes at 1 mole. Kg^{-1} of water. The thermodynamic equilibrium constant for the dissolution reaction (Eq. 5) in a molality basis can be written as

$$\ln K^\circ = -\frac{\mu^\circ_{iaq} - \mu^\circ_{ig}}{RT} = \ln \frac{m_i \gamma_i}{P\, \emptyset_{ig}\, y_i} \tag{7}$$

At the limit of an infinitely dilute solute, the aqueous solution becomes ideal and γ_i reaches 1. Also, for a binary-mixture, φ becomes φ_g^∞, that is the fugacity coefficient of solute at infinite dilution (Akinfiev and Diamond, 2003). Also, because Henry's constant is commonly used to express solubilities, we can use the relation by Prausnitz et al. (1986) to obtain the following

$$k_H = \frac{N_w}{K^\circ} = \frac{P\, \emptyset_g^\infty\, y_i}{m_i / N_w} \tag{8}$$

where N_w is a conversion factor from molality to concentration that is equal to 55.1 mol. kg^{-1} , and is the reciprocal of H_2O molecular weight (Akinfiev and Diamond, 2003). Additionally, Akinfiev and Diamond (2003) assumed that for an infinitely dilute gas y_i can be approximated as m_i/N_w. This approximation was only necessary to simplify Eq. 7 further to

$$k_H = \frac{N_w}{K^\circ} = P\, \emptyset_g^\infty \tag{9}$$

To get φ_g^∞ and y_i in a multi-component gas phase, any EoS can be used with a Gibbs minimization solver. In the special case of a binary-mixture or black oil framework, y_i can be approximated as 1- y_{H2O} if the solution is saturated. The mole fraction y_{H2O} may be obtained from Rauolt's law for ideal liquids. This approach was validated up to up to 180 °C, 100 MPa, and salinity of 6 mol/kg w (Kerkache et al. (2024) and Tawil et al., (2024)). Otherwise, when the solution is undersaturated, y_i is approximated as 1.

2.2.1 Salting-out Correction

When the water includes a salt such as NaCl, intermolecular interactions with the gas reduces its solubility and this is known as salting out. This effect is usually incorporated into the gas activity coefficient. To model the salting-out effect in a H_2–H_2O–NaCl system, Chabab et al. (2024) and Zhu et al. (2022) implemented a Pitzer activity coefficient model whereas Torin-Ollarves et al. (2021) and Kerkache et al. (2024) developed a temperature- and salinity-dependent Sechenov coefficient (k_s) for the activity coefficient model. Also, Tawil et al., (2024) applied a Sechenov activity coefficient successfully to dissolution of hydrogen and methane mixture in brine. In all these studies, a linear proportionality between salinity, represented by the ionic strength I_s, and activity coefficient was adequate to fit the solubility data, as the following

$$ln\gamma_{H_2} = \ln\left(\frac{x_{H_2,w}}{x_{H_2,b}}\right) = k_s I_s \tag{10}$$

Where w and b subscripts refer to pure water and brine phases.

2.2.1 Correction for high-pressure condition of aqueous Phase

When system pressure is above the water saturated pressure, the non-ideality of the aqueous phase needs to be corrected. A Poynting factor (Π_i) within a Krichevesky-Kasarnovsky scheme can be implemented in the equilibrium condition (Eq. 7) as

$$k_H = \frac{P\, \emptyset_{ig}^\infty\, y_i}{m_i / N_w \gamma_i\, \Pi_i} \tag{11}$$

where the Poynting factor for any component *i* is defined as

$$\Pi_i = \exp\left[\frac{v^\infty_{m,H_2(aq)}}{RT}(P_w - P_w^{sat})\right] \tag{12}$$

In Eq. 11, $v^{\infty}_{m,\,H2(aq)}$ is the partial molar volume of the infinitely dilute aqueous hydrogen. The difference between P_w and P_w^{sat} represents the increase in solvent pressure above saturation conditions. Torin-Ollarves et al. (2021) and Kerkache et al. (2024) applied the Krichevesky-Kasarnovsky scheme successfully to match their experimental and molecular simulation solubility data up to 180 °C, 100 MPa and salinity of 6 mol/kg w.

For high-temperature geothermal applications above approximately 150 °C, the Krichevesky–Kasarnovsky method becomes unreliable because it assumes an incompressible partial molar volume in the Poynting factor (Kishima and Sakai, 1984). At higher pressures, the increased solubility of hydrogen may also invalidate the assumption of an infinitely dilute gas, thereby undermining the premise that the H_2 activity coefficient equals 1 in pure water. Even below the critical point of water (374 °C, 22.064 MPa), Kerkache et al. (2024) found that the method's assumptions may not hold.

Specifically, in their Poynting factor formula, both Kerkache et al. (2024) and Torin-Ollarves et al. (2021) used an apparent molar volume of about 19 $cm^3\ mol^{-1}$ at 25 °C and 0.1 MPa to fit experimental solubility data. These values are much lower than the 23.1–26 $cm^3\ mol^{-1}$ measured directly under the same conditions (Plyasunov et al., 2018). Obtaining accurate values of apparent molar volume is important not only for predicting hydrogen's thermodynamic properties in supercritical water with moderate to high densities (>300 kg m^{-3}) but also for calculating transport properties such as density and viscosity (Plyasunov et al., 2018).

In these solubility models, however, the discrepancy in molar volume is largely compensated for by the activity coefficient that may itself be inaccurate because the assumption of an ideal liquid at zero salinity no longer applies. Consequently, although these approaches match experimental solubilities reasonably well, the individual values for apparent molar volume and the activity coefficient may not accurately reflect their true behavior.

2.2.2 Extension to Near and Supercritical Region

The Helgeson–Kirkham–Flowers (HKF) equation of state introduced by Tanger and Helgeson (1988) accurately predicts the thermodynamic properties of aqueous ions over a wide range of temperatures (0–600 °C) and pressures (1–5000 bar). Owing to its popularity in the geochemical community, it is available through the *supercrtbl* database (Johnson et al., 1992; Zimmer et al., 2016). Attempts to extend HKF to neutral aqueous species (Shock et al., 1989; Schulte et al., 2001) have uncovered inaccuracies near and above the critical point of water (O'Connell et al., 1996; Plyasunov and Shock, 2001b).

To address these issues, Akinfiev and Diamond (2003) proposed a new equation of state (EoS) for predicting thermodynamic properties of gases (e.g., H_2) at infinite dilution in water from 0 to 500 °C and 0.1 to 200 MPa, improving upon the semiempirical model of Japas and Levelt Sengers (1989). Their predictions are based on the virial EoS, along with a temperature- and pressure-dependent empirical correlation for the second virial coefficient (*B*). To better capture the dissolved gas volume in water, they included a scaling factor for H_2O. This EoS is compatible with the HKF model and is accessible via the *thermofun* database (Miron et al., 2023). For hydrogen, it successfully reproduces experimental Henry's coefficient under saturated pressure conditions (Kerkache et al., 2024) and near the water critical point using Kishima and Sakai (1984) experiments (Bazrakina et al., 2020). Improved accuracy compared to the HKF EoS in near- and supercritical, low-density water by modeling graphite solubility (producing CO_2 and CH_4) was demonstrated by Akinfiev and Diamond (2003), where their predictions correctly approached the ideal gas limit. ~~For saturated-pressure condition,~~

Despite these successes, the Akinfiev and Diamond model is largely based on phenomenological fits to low-density data, reflecting limited experimental information on hydrogen solubility in compressed supercritical water. Consequently, the model may be less reliable at moderate (300–900 kg m^{-3}) and high (>1000 kg m^{-3}) water densities (Plyasunov et al., 2018). Indeed, at isotherms of 726 °C and 1226 °C, once water density exceeds about 250 kg m^{-3}, Plyasunov et al. (2018) predict higher fugacity coefficients than Akinfiev and Diamond (2003). This discrepancy means that the Akinfiev and Diamond model likely underestimates Henry's coefficient and overestimates solubilities, given their direct relationship.

To broaden the applicability of fugacity coefficient and molar volume models for H_2 in water, Plyasunov et al. (2018) introduced an alternative framework that covers water densities from 0 to 1500 kg m^{-3}. They used the dimensionless A^{∞}_{12} function and its complement C^{∞}_{12}, that are referred to as integrals of the solute–solvent direct correlation function (DCFI) at infinite dilution (O'Connell, 1971), thereby avoiding numerical issues near the critical point and at zero water density. Their approach employs a virial-type model at low water densities, similar to Akinfiev and Diamond (2003), and switches to hard-sphere mixture equations at higher densities, bridging these regimes with a corresponding-states correlation. As evidence of its robustness, Plyasunov et al. (2018) matched fugacity coefficient data from Kishima and Sakai (1984). Under highly compressed, supercritical conditions (726 °C and 1226 °C), their model predicts hydrogen fugacity higher than the Akinfiev and Diamond (2003) EoS, that appears biased toward low-density regions. According to Eq.7, this implies that Akinfiev and Diamond (2003) model would overestimate hydrogen solubility compared to Plyasunov et al. (2018). This is an outcome that underscores the need for more experimental data at moderate and high densities and improved models.

4. RESULTS

4.1 Hydrogen and pure water

There are several experiments that have hydrogen solubility related data at hydrothermal conditions. We used Kishima and Sakai (1984) experiments to test three different models in the literature because they were the most comprehensive, i.e. temperature from 569 to 760.15 K, pressure from 9.8 to 99.9 MPa and water density range from roughly 200 kg m^3 to 800 kg m^3. The appendix shows three selected solubility isotherms from Kishima and Sakai (1984) versus pressure and water density. The other datasets that measured hydrogen

solubility at supercritical conditions, such as Shaw (1963), Eklund et al. (1997) and Moss & Was (2014) were discarded because they exhibited high scatter of Henry's coefficient, up to 50% or the tested water density range was very limited to low values below 300 kg m^{-3}.

Kishima and Sakai (1984) conducted hydrothermal experiments of a magentite-hematite-water (MHW) mineral buffer. Buffer experiments are important for understanding stability conditions of oxides in rock minerals. In these experiments, the oxygen and/or hydrogen are generated by imposing specific temperature and pressure on the mineral in solution. In the MHW buffer, the reactions involved are

$$\text{Hematite } (Fe_2O_3) \leftrightarrow \tfrac{1}{2}\, O_{2(g)} + 2\text{Magnetite } (Fe_3O_4) \tag{13}$$

and

$$H_{2(g)} + \tfrac{1}{2}\, O_{2(g)} \leftrightarrow H_2O_{(l)} \tag{14}$$

that are combined to

$$\text{Hematite } (Fe_2O_3) + H_{2(g)} \leftrightarrow 2\text{Magnetite } (Fe_3O_4) + H_2O_{(l)} \tag{15}$$

We used Henry's coefficient and hydrogen solubility to predict the accuracy of three different models: Akinfiev & Diamond (2003) EoS, HKF EoS and Plyasunov et al. (2018). We only used Akinfiev & Diamond (2003) EoS, HKF EoS to predict solubility. We chose these parameters because solubility is not enough to determine accuracy as pointed out in section 2.2.1. In order to convert fugacity coefficient in Plyasunov et al. (2018) to Henry's coefficient, we used Eq. 9. For Akinfiev & Diamond (2003) EoS and HKF EoS, we followed a procedure similar to Scheuermann et al. (2020). Specifically, the reaction constant for the reaction in Eq. 14 can be obtained from each database at every temperature and pressure condition and related to activity through the expression (Frost (1991)

$$K^{\circ} = \frac{a_{H_2O} \cdot a_{Magnetite}}{a_{Hematite} \cdot a_{H_2}} \tag{16}$$

By assuming pure mineral and water phases and standard fugacity of hydrogen at 1 bar, Eq. 15 simplifies to

$$f_{H_2} = \frac{1}{K^{\circ}} \tag{17}$$

that can be converted into fugacity-concentration ratio (Y_{H2}) using Kishima and Sakai (1984) as

$$Y_{H_2} = \frac{f_{H_2}}{m_{H_2}} \tag{18}$$

where m_{H2} is obtained using the equilibrium solver in reaktoro of the reaction in Eq. 14. Y_{H2} can then be converted into Henry's coefficient using:

$$k_H = N_w\, Y \tag{19}$$

For Kishima and Sakai (1984) experiments, we converted their tabulated Y_{H2} into Henry's coefficient using:

$$k_H[bar] = 1244.13\, Y[bar.cm^{-3}.g] \tag{20}$$

Figure 2 shows prediction results of Henry's coefficient and hydrogen solubility. Unlike solubility below the water critical point, hydrogen solubility increases with temperature at conditions near and above the water critical point. On the other hand, because Henry's coefficient is inversely related to solubility (Eq. 9), it would decrease with increasing temperatures.

From Figure 2, we see that Akinfiev & Diamond (2003) EoS and Plyasunov et al. (2018) perform better compared to HKF EoS. Because fugacity is controlled in these experiments, the absolute deviation error is not an appropriate criteria for comparing performance of different models. Rather, the rate of change of Henry's coefficient with respect to pressure is a more representative metric as shown in Figure 3. The parity plot in Figure 3 shows that HKF tends to overestimate the rate of change of Henry's coefficient with respect to pressure while Akinfiev & Diamond (2003) EoS did the opposite. On the other hand, Plyasunov et al. (2018) predictions of changes in Henry's coefficient with pressure were the most balanced.

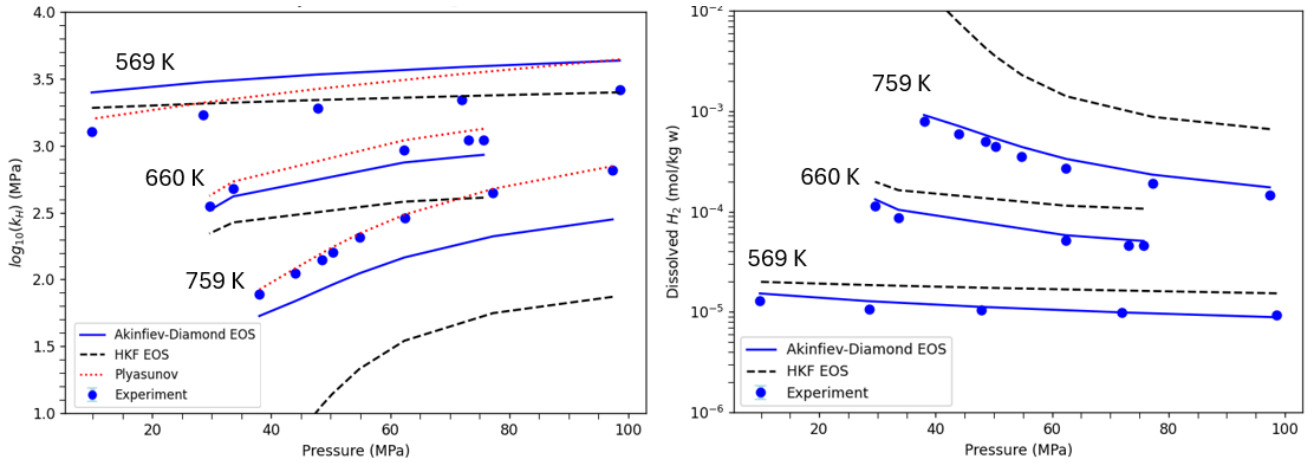

Figure 2: Modelling Henry's coefficient (left) and hydrogen solubility (right) and from Kishima and Sakai (1984) experiments in MHW system using Akinfiev & Diamond (2003) EoS, HKF EoS and Plyasunov et al. (2018).

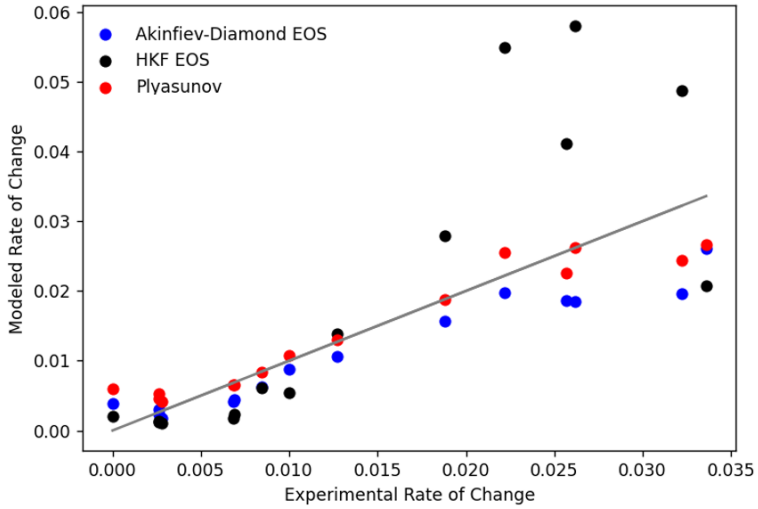

Figure 3: Parity plot to compare rate of change in Henry's coefficient at 569, 660, and 759 K among the different models (Akinfiev & Diamond (2003) EoS, HKF EoS and Plyasunov et al. (2018)) and Kishima and Sakai (1984) experiments

4.2 H_2-KCl-H_2O

To evaluate the impact of salting out on hydrogen solubility at super-critical conditions, we used Scheuermann et al. (2020) experiments on the magnetite-hematite mineral buffer in KCl solution. In these experiments, when the single-phase buffer solution split into a vapor and liquid phase, hydrogen solubility and ionic strength measurements were conducted on the vapor phase only while the liquid phase was discarded.

Figure 4 shows two isotherms at 673 and 723 K using Akinfiev and Diamond (2003) and HKF EoS. The phase type of either vapor or single phase was tabulated in Scheuermann et al. (2020) experiments. Also, the phase change is distinguished by the quality of the model fitting due to salting-out effect. Specifically, because the single-phase fluid contained higher salinity compared to the vapor phase, salting-out was more evident, and led to lower gas solubility compared to model prediction. Because neither EoS incorporates salting-out effects in their activity coefficient, we implemented a Sechenov-type model similar to Eq. 10.

Figure 5 shows matching results using a Sechenov coefficient of 0.6, that was determined through trial and error because the Sechenov coefficient is usually measured at conditions below the critical point of water. Recently, Kerkache et al. (2024) and Torín-Ollarves & Trusler (2021) developed temperature-salinity and temperature dependent Sechenov coefficients for hydrogen storage conditions, respectively. Under hydrogen storage conditions, their Sechenov coefficients are always below 0.22 (Kerkache et al. (2024)) and 0.3 (Torín-Ollarves & Trusler (2021)). Appendix shows Sechenov coefficients by Kerkache et al. (2024) versus temperature for 0.8 and 1 molal, which are the maximum salinities recorded in the Scheuermann et al. (2020) experiments. If the Sechenov coefficient of Kerkache et al. (2024) is extended to conditions of temperature and salinity of the single-phase regions in isotherms in Figures 4 and 5, it would predict values between 0.34 to 0.4 that are close to our matching value of 0.6. Also, given that the salinities in the experiments are very

low (maximum of 1 Molal), it is expected that salting-out is not very significant and requires Sechenov coefficients on the higher end. Additional experiments using high salinity super-critical water are required to accurately model salting out.

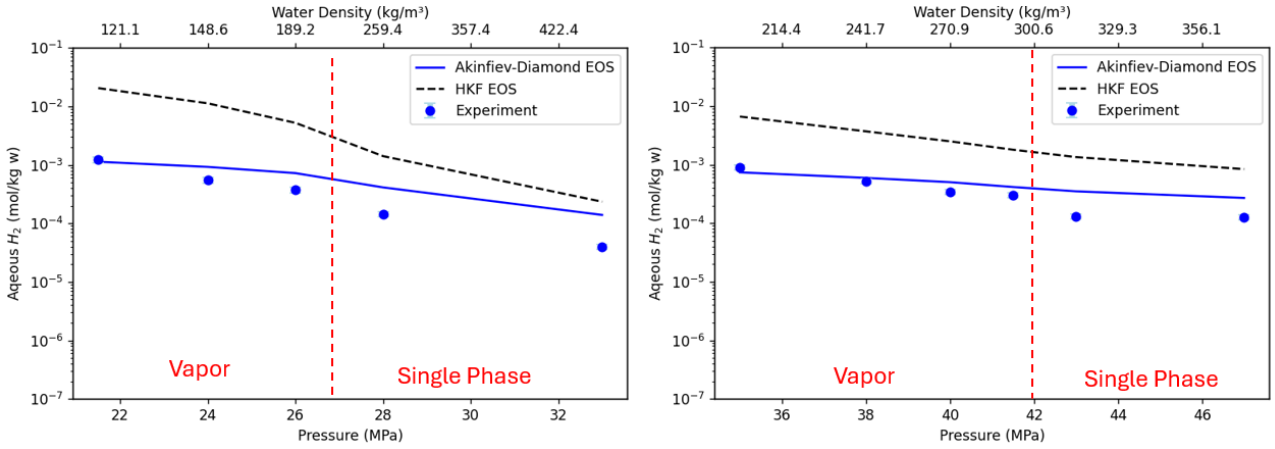

Figure 4: Modelling solubility isotherms from Scheuermann et al. (2020) experiments of magnetite-hematite in KCl solution. On the left, solubility at 673 K and salinity that increases from 0.01 (vapor phase) to 1 molal (single-phase). On the right, solubility at 723 K and salinity that increases from 0.04 (vapor phase) to 0.8 molal (single-phase).

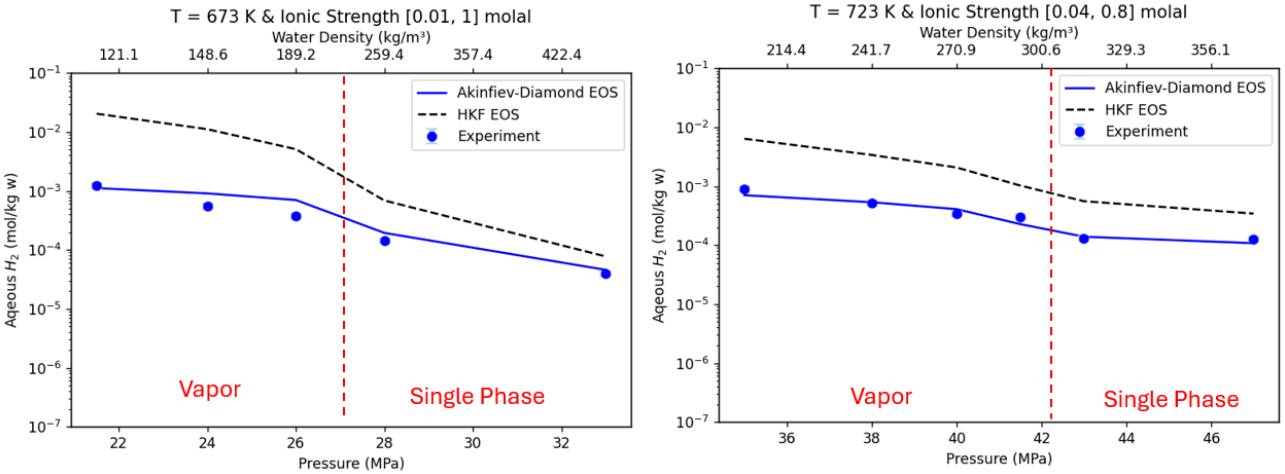

Figure 5: Solubility isotherms from figure 4 after applying Sechenov coefficient of 0.6 to account for salting-out effect in the single-phase region and match experimental data. On the left, 673 K and salinity that increases from 0.01 (vapor phase) to 1 molal (single-phase). On the right, 723 K and salinity that increases from 0.04 (vapor phase) to 0.8 molal (single-phase).

5. CONCLUSION

Accurate modeling of hydrogen solubility is critical for understanding the generation and transport of hydrogen in hydrothermal systems, particularly in environments near or above the critical point of water. In this study, we compared the Helgeson–Kirkham–Flowers (HKF) EoS, the Akinfiev and Diamond (2003) EoS, and the Plyasunov et al. (2018) predictions of hydrogen's Henry's coefficient and solubility against available experimental data. Both the Akinfiev and Diamond (2003) and Plyasunov et al. (2018) models offered more accurate predictions of hydrogen solubility and Henry's coefficients than HKF, especially in near-critical and supercritical conditions. None of the models, however, adequately captured salting-out effects under saline conditions. Our analysis revealed that a Sechenov coefficient between 0.4 to 0.6 captures the salting-out effect up to salinity of 1 molal. Additional experiments are required at higher salinities to evaluate salting-out effects at super-critical conditions.

NOMENCLATURE

μ	chemical potential
μ°	standard molar chemical potential

R	gas constant
T	temperature
f	fugacity
l	liquid phase
g	gaseous phase
aq	aqueous phase
x	liquid molar fraction
y	gas molar fraction
P	pressure
φ	fugacity coefficient
m	species molality in the aqueous phase
γ	species activity coefficient in a molality basis
k	k-value constant
$k_{H,}$	Henry's constant
K°	reaction constant
a	activity
N_w	conversion factor from molality to concentration that is equal to 55.1 mol. kg^{-1}
k_s	Sechenov coefficient
I_s	ionic strength
Π	Poynting factor
$v^{\infty}_{m,}$	partial molar volume of the infinitely dilute aqueous species
P_w^{sat}	saturation pressure of water
P_w	water pressure
Y	fugacity-concentration relationship

REFERENCES

Akinfiev, N. N., & Diamond, L. W. (2003). Thermodynamic description of aqueous nonelectrolytes at infinite dilution over a wide range of state parameters. *Geochimica et Cosmochimica Acta*, 67(4), 613-629. https://doi.org/10.1016/S0016-7037(02)01141-9.

Bazarkina, E. F., Chou, I. M., Goncharov, A. F., & Akinfiev, N. N. (2020). The behavior of H2 in aqueous fluids under high temperature and pressure. *Elements*, 16(1), 33-38. https://doi.org/10.2138/gselements.16.1.33.

Charlou, J. L., Donval, J. P., Konn, C., Ondreas, H., Fouquet, Y., Jean-Baptiste, P. & Fourré, E. (2010). High production and fluxes of H2 and CH4 and evidence of abiotic hydrocarbon synthesis by serpentinization in ultramafic-hosted hydrothermal systems on the Mid-Atlantic Ridge. In Rona, P. A., Devey, C. W., Dyment, J., & Murton, B. J. (Eds.), *Diversity of Hydrothermal Systems on Slow Spreading Ocean Ridges* (pp. 265-295). American Geophysical Union Monograph Series 188.

Chabab, S., Kerkache, H., Bouchkira, I., Poulain, M., Baudouin, O., Moine, É., Ducousso, M., Hoang, H., Galliéro, G., & Cézac, P. (2024). Solubility of H2 in water and NaCl brine under subsurface storage conditions: Measurements and thermodynamic modeling. *International Journal of Hydrogen Energy*, 50, Part B, 648-658. https://doi.org/10.1016/j.ijhydene.2023.10.290.

Chabab, S., Théveneau, P., Coquelet, C., Corvisier, J., & Paricaud, P. (2020). Measurements and predictive models of high-pressure H2 solubility in brine (H2O+NaCl) for underground hydrogen storage application. *International Journal of Hydrogen Energy*, 45(56), 32206-32220.

Churakov, S. V., & Gottschalk, M. (2003a). Perturbation theory-based equation of state for polar molecular fluids: II. Fluid mixtures. *Geochimica et Cosmochimica Acta*, 67(13), 2415-2425. https://doi.org/10.1016/S0016-7037(02)01348-0.

Churakov, S. V., & Gottschalk, M. (2003b). Perturbation theory-based equation of state for polar molecular fluids: I. Pure fluids. *Geochimica et Cosmochimica Acta*, 67(13), 2397-2414. https://doi.org/10.1016/S0016-7037(02)01347-9.

Eklund, K., Lvov, S. N., & Macdonald, D. D. (1997). The measurement of Henry's constant for hydrogen in high subcritical and supercritical aqueous systems. *Journal of Electroanalytical Chemistry*, 437(1-2), 99-110.

Frost, B. (1991). Introduction to oxygen fugacity and its petrologic importance. In D. Lindsley (Ed.), *Oxide Minerals: Petrologic and Magnetic Significance* (pp. 1-10). Berlin, Boston: De Gruyter. https://doi.org/10.1515/9781501508684-004.

Japas, M. L., & Sengers, J. L. (1989). Gas solubility and Henry's law near the solvent's critical point. *AIChE Journal*, 35(5), 705-713.

Johnson, J. W., Oelkers, E. H., & Helgeson, H. C. (1992). SUPCRT92 - A software package for calculating the standard molal thermodynamic properties of minerals, gases, aqueous species, and reactions from 1-bar to 5000-bar and 0°C to 1000°C. *Computers & Geosciences*, 18(7), 899-947.

Kiemde, A. F., Ferrando, N., de Hemptinne, J.-C., Le Gallo, Y., Reveillère, A., & Roa Pinto, J. S. (2023). Hydrogen and air storage in salt caverns: A thermodynamic model for phase equilibrium calculations. *Science & Technology for Energy Transition*, 78. https://doi.org/10.2516/stet/2023004.

Kerkache, H., Hoang, H., Cézac, P., Galliéro, G., & Chabab, S. (2024). The solubility of H2 in NaCl brine at high pressures and high temperatures: Molecular simulation study and thermodynamic modeling. *Journal of Molecular Liquids*, 400(2024), 124497. https://doi.org/10.1016/j.molliq.2024.124497.

Kishima, N., & Sakai, H. (1984). Fugacity-concentration relationship of dilute hydrogen in water at elevated temperature and pressure. *Earth and Planetary Science Letters*, 67(1), 79-86. https://doi.org/10.1016/0012-821X(84)90040-2.

Klein, F., Tarnas, J., & Bach, W. (2020). Abiotic sources of molecular hydrogen on Earth. *Elements*, 16(1), 19-24.

Leal, A. M. M. (2015). Reaktoro: An open-source unified framework for modeling chemically reactive systems. https://reaktoro.org.

Miron, et al. (2023). ThermoFun: A C++/Python library for computing standard thermodynamic properties of substances and reactions across wide ranges of temperatures and pressures. *Journal of Open Source Software*, 8(83), 4624. https://doi.org/10.21105/joss.04624.

Moss, T., & Was, G. S. (2014). Determination of the nickel/nickel oxide phase transition and Henry's constant in hydrogenated subcritical and supercritical water. *Journal of The Electrochemical Society*, 162(1), C35.

O'Connell, J. P. (1971). Thermodynamic properties of solutions based on correlation functions. *Molecular Physics*, 20(1), 27-33. https://doi.org/10.1080/00268977100100031.

O'Connell, J. P., Sharygin, A. V., & Wood, R. H. (1996). Infinite dilution partial molar volumes of aqueous solutes over wide ranges of conditions. *Industrial & Engineering Chemistry Research*, 35(8), 2808-2812.

Plyasunov, A. V., & Bazarkina, E. F. (2018). Thermodynamic properties of dilute hydrogen in supercritical water. *Fluid Phase Equilibria*, 470, 140-148. https://doi.org/10.1016/j.fluid.2017.11.004.

Plyasunov, A. V., & Shock, E. L. (2001). Correlation strategy for determining the parameters of the revised Helgeson-Kirkham-Flowers model for aqueous nonelectrolytes. *Geochimica et Cosmochimica Acta*, 65(21), 3879-3900.

Prausnitz, J. M., Lichtenthaler, R. N., & De Azevedo, E. G. (1998). *Molecular thermodynamics of fluid-phase equilibria* (3rd ed.). Pearson Education.

Scheuermann, Xing, Ding, & Seyfried. (2020). Experimental measurement of H2(aq) solubility in hydrothermal fluids: Application to the Piccard hydrothermal field, Mid-Cayman Rise. *Geochimica et Cosmochimica Acta*, 283, 22-39. https://doi.org/10.1016/j.gca.2020.05.020.

Schulte, M. D., Shock, E. L., & Wood, R. H. (2001). The temperature dependence of the standard-state thermodynamic properties of aqueous nonelectrolytes. *Geochimica et Cosmochimica Acta*, 65(21), 3919-3930.

Shock, E. L., Helgeson, H. C., & Sverjensky, D. A. (1989). Calculation of the thermodynamic and transport properties of aqueous species at high pressures and temperatures: Standard partial molal properties of inorganic neutral species. *Geochimica et Cosmochimica Acta*, 53(9), 2157-2183.

Shaw, H. R. (1963). Hydrogen-water vapor mixtures: control of hydrothermal atmospheres by hydrogen osmosis. *Science*, 139(3560), 1220-1222.

Tawil, M., Borello, E. S., Bocchini, S., Pirri, C. F., Verga, F., Coti, C., Scapolo, M., Barbieri, D., & Viberti, D. (2024). Solubility of H2-CH4 mixtures in brine at underground hydrogen storage thermodynamic conditions. *Frontiers in Energy Research*, 12:1356491. https://doi.org/10.3389/fenrg.2024.1356491.

Torín-Ollarves, G. A., & Trusler, J. M. (2021). Solubility of hydrogen in sodium chloride brine at high pressures. *Fluid Phase Equilibria*, 539, 113025.

Zhu, Z., Cao, Y., Zheng, Z., & Chen, D. (2022). An accurate model for estimating H2 solubility in pure water and aqueous NaCl solutions. *Energies*, 15(14), 5021. https://doi.org/10.3390/en15145021.

Zimmer, K., Zhang, Y. L., Lu, P., Chen, Y. Y., Zhang, G. R., Dalkilic, M., & Zhu, C. (2016). SUPCRTBL: A revised and extended thermodynamic dataset and software package of SUPCRT92. *Computers & Geosciences*, 90, 97-111. https://doi.org/10.1016/j.cageo.2016.02.013.

APPENDIX

Sechenov coefficients by Kerkache et al. (2024) vs. temperature for 0.8 and 1 molal

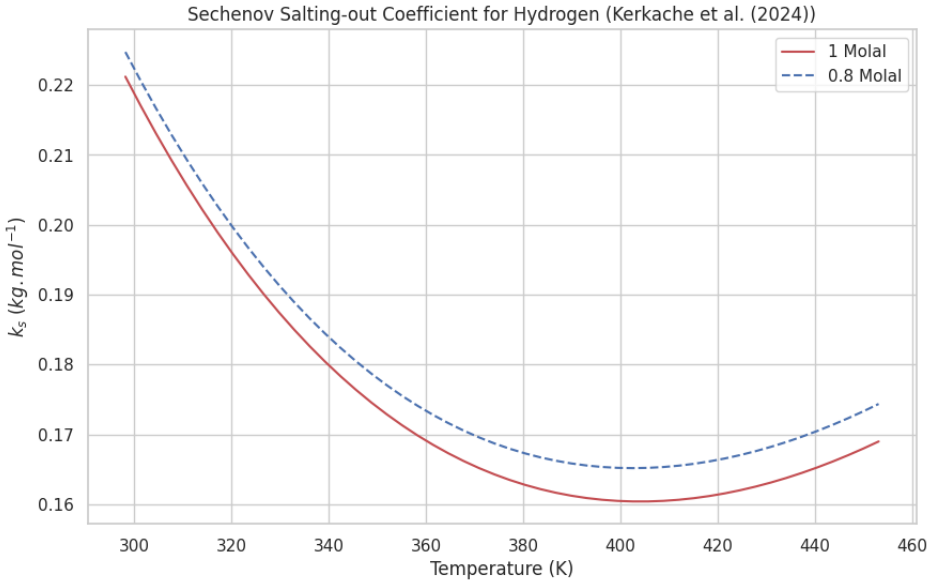

Henry's coefficient and solubility isotherms at three temperatures near and supre-critical.

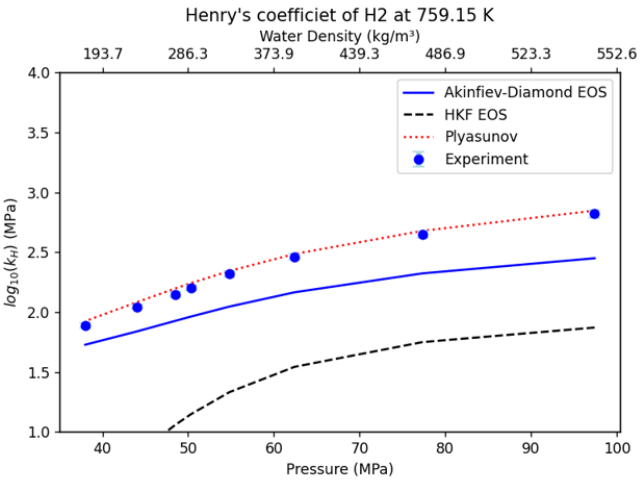

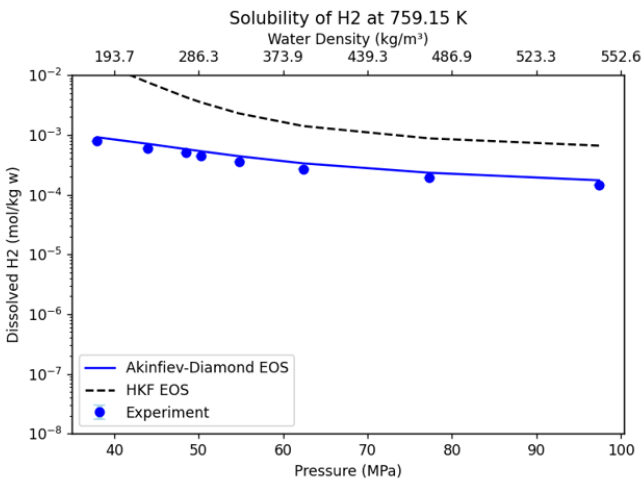

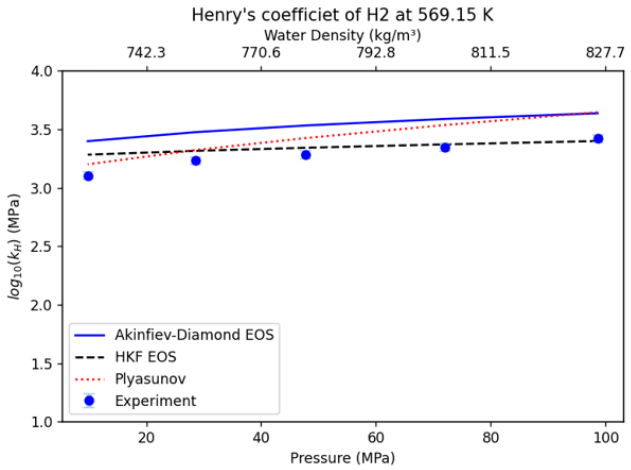
Henry's coefficiet of H2 at 569.15 K
Water Density (kg/m³)
742.3
770.6
792.8
811.5
827.7
$log_{10}(k_H)$ (MPa)
Pressure (MPa)
Akinfiev-Diamond EOS
HKF EOS
Plyasunov
Experiment

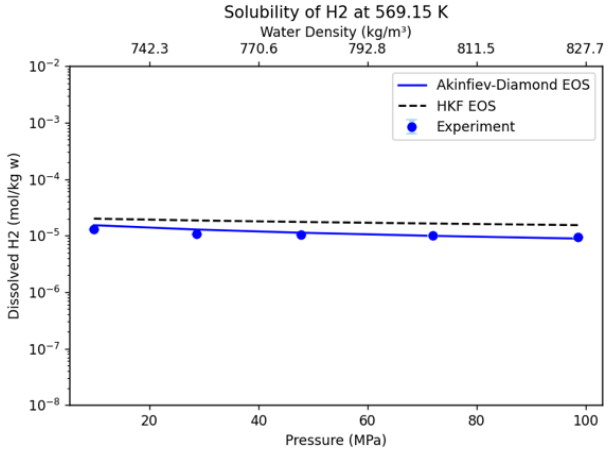
Solubility of H2 at 569.15 K
Water Density (kg/m³)
742.3
770.6
792.8
811.5
827.7
Dissolved H2 (mol/kg w)
Pressure (MPa)
Akinfiev-Diamond EOS
HKF EOS
Experiment

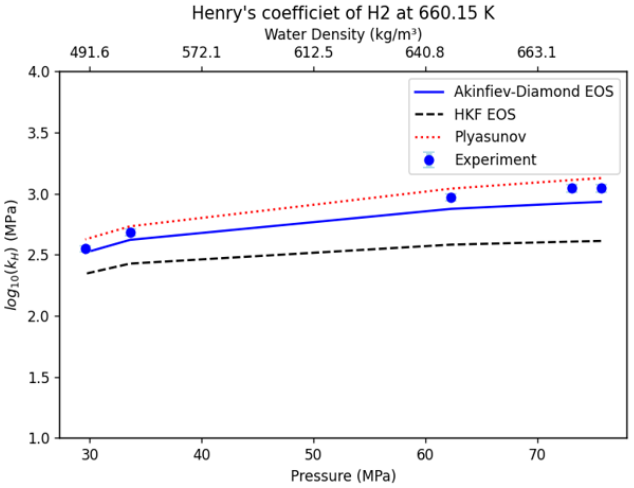
Henry's coefficiet of H2 at 660.15 K
Water Density (kg/m³)
491.6
572.1
612.5
640.8
663.1
$log_{10}(k_H)$ (MPa)
Pressure (MPa)
Akinfiev-Diamond EOS
HKF EOS
Plyasunov
Experiment

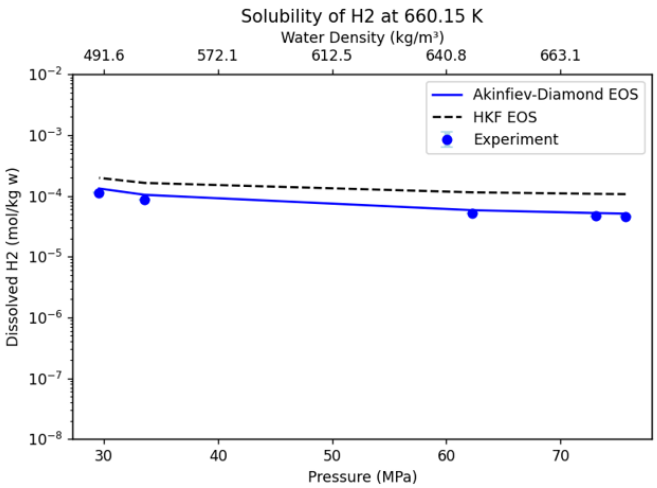
Solubility of H2 at 660.15 K
Water Density (kg/m³)
491.6
572.1
612.5
640.8
663.1
Dissolved H2 (mol/kg w)
Pressure (MPa)
Akinfiev-Diamond EOS
HKF EOS
Experiment